Effects of Swirl on Intermittency Characteristics in Non-Premixed Flames

Combustion Science and Technology, 2012, Volume 184, Issue 5, pp629-659

K.K.J.Ranga Dinesh, K.W.Jenkins

School of Engineering, Cranfield University, Cranfield, Bedford, MK43 0AL, UK

Corrosponding Author: Ranga.Dinesh@Cranfield.ac.uk (+44 (0) 1234 750111)

Keywords: Intermittency, Swirl, Combustion, Non-Premixed, LES

Abstract

Swirl effects on velocity, mixture fraction and temperature intermittency have been analysed for turbulent methane flames using LES. The LES solves the flitered governing equations on a structured Cartesian grid using a finite volume method, with turbulence and combustion modelling based on the localised dynamic Smagorinsky model and the steady laminar flamelet model respectively. Probability density function (pdf) distributions demonstrate a Gaussian shape closer to the centreline region of the flame and a delta function at far radial position. However, non-Gaussian pdfs are observed for velocity and mixture fraction on the centreline in a region where centre jet precession occurs. Non-Gaussian behaviour is also observed for the temperature pdfs close to the centreline region of the flame. Due to the occurrence of recirculation zones, the variation from turbulent to non turbulent flow is more rapid for the velocity than the mixture fraction and therefore indicates how rapidly turbulence affects the molecular transport in these regimes of the flame. The present findings indicate a requirement for improved sub-grid scale modelling for LES and potentially a separate intermittency scaling allowance for the scalar and velocity fields.

1 Introduction

Swirling flames are commonly used in a variety of practical combustion systems, including diesel and gas turbine engines and industrial furnances [31, 45]. Recirculation zones and vortex breakdown (VB) regions are usually found in many turbulent swirling flames and it is well known that swirl stabilised flames are effective in providing a source of well mixed combustion products and acts as storage of heat and chemically active species to sustain combustion [16, 19]. Precession motion and precessing vortex core (PVC) structures also occur with certain conditions in swirling flows [44]. Investigation of the intermittency in a turbulent swirling flame is particularly interesting due to the different flow structures and various mixing rates that directly effect to form different regimes in a turbulent flame. Particularly, unconfined turbulent swirling flames display an intermittent behaviour in some regions such as inside the recirculation zones and close to the outer edge where flow alternates between turbulent and irrotational states (external intermittency) and also due to differences of energy or scalar dissipation rates (internal intermittency). Mathematically an indicative function can be used to identify the external intermittency in a way such that it has a value of one in the turbulent region and zero in the irrotational region. In other words, external intermittency represents the fraction of time during which a point is inside the turbulent field. The dividing interphase between turbulent and laminar regions in a turbulent flame is sharp and constantly distorted by different size of turbulent eddies, with turbulent flame propagating into the irrotational region while laminar fluid is entrained into the turbulent region. Therefore study of intermittency in swirling flames is important and challenging due to the nature of multi-scale and multi-physics environment.

Numerous experimental, theoretical and numerical investigations for turbulent intermittency have been carried out for both reacting and non-reacting applications in fairly simple geometries. Townsend [46] has taken the first intermittency measurements for a turbulent wake generated by a circular object and a similar technique was also used by

Corrsin and Kistler [9] to measure the intermittency in a round jet and by Klebanoff [28] in a boundary layer with zero pressure gradient. Wygnanski and Fielder [48] recorted the measurements for a jet using velocity gradients with respect to time and similar technique also applied by Chevray and Tutu [7] to measure the intermittency of a jet. However, Bilger [3] proposed a method using probability density functions (pdf) to overcome some of the difficulties encountered for calculation of intermittency by previous investigators and later Nakamura et al. [35], and Schefer and Dibble [47] adopted Bilger's method to evaluate intermittency for their experiments. Major theoretical work on intermittent flows have been initially carried out by Libby [2], Dopazo [15], and Chevray and Tutu [7]. Later, Sreenivasan [43], Jimenez [21], Gibbson and Doering [17] and Li and Meneveau [49] also derived various theoretical explanations for turbulent intermittency.

Although the majority of turbulence models currently in use were derived for fully developed flows, few groups have developed and applied Reynolds Averaged Navier-Stokes (RANS) based intermittency models especially for non-reacting turbulent jets. For example, a $k-\epsilon$ model based intermittency model was developed by Byggstoyl and Kollomann [6] and Kollmann and Janicka [29] who studied intermittency using the transport pdf. Cho and Chung [8] developed a more economical intermittency model by incorporating an intermittency transport equation into an already existing $k-\epsilon$ turbulence model. Few groups extended the Cho and Chung [8] intermittency model applying it to different applications such as axisymmetric plume [10], and a plane plume [22]. Pope [40] also calculated intermittency using velocity-composition transported probability density function.

Despite the success of various modelling efforts on turbulent combustion, Kerstein [25] outlined many important modelling challenges of turbulence in the combustion processes. As explained by Kerstein [25], there are certain areas in turbulent combustion which require additional focus that are either poorly understood or not sufficiently represented by present models. Intermittency is one such topic that involves several unresolved fundamental issues with regard to the representation of turbulence effects in combustion

models for both turbulent non-premixed and premixed combustion. The combination of Kerstein's findings and computational advances now being made in swirl combustion highlight the need for further studies of intermittency modelling in which little is known to date.

In recent years considerable advances have been made toward modelling of swirl combustion systems using large eddy simulation (LES) technique for various engineering configurations. For example, Huang et al. [20] carried out LES on combustion dynamics for a gas turbine swirl injector and Pierce and Moin [36] also performed LES of swirling flames. Di Mare et al. [11] and Kim and Syred [26] studied LES for model swirl combustors while Selle et. al. [41] performed LES for industrial gas turbine burner. Grinstein and Fureby [18] also performed LES for one of the General Electric swirl combustors while Mahesh et al. [32] carried out LES for a section of Pratt and Whitney combustor. Moreover, Boudier et al. [4] performed the LES calculations of isothermal and reacting flows in a simplified ramjet combustor.

Despite having carried out broad LES investigations for complex swirling flames, the physical interpretation of intermittent characteristics for turbulence and mixing are not well understood. Therefore the work described in this paper represents an investigation on the effects of swirl on intermittency characteristics of turbulent unconfined non-premixed swirling flames. The objective is to examine the effects of swirl on intermittent behaviour of velocity, mixture fraction and temperature at identified important regimes in swirling non-premixed flames.

The swirl burner used in this work is the Sydney burner [1, 23, 34], which is frequently used in modelling of unconfined swirling flames. Our previous LES investigations targeted some of the Sydney flames for LES validation [24] and instability analysis [13]. This work selected an experimental pure methane swirling flame (SM1) with swirl number 0.5 as a base while creating another two numerical flames with increased swirl numbers 0.75 and 1.0. The discussion focuses on the probability density functions (pdfs) and radial

profiles of intermittency for velocity, mixture fraction and temperature behaviour respect different swirl numbers. This paper is organised as follows: Section 2 describes the swirl burner experimental details and then followed by the theoretical formulations and modelling in section 3. In section 4 we discuss the numerical computation followed by the results and discussion in section 5. We summarise the conclusions in section 6 and suggest future work.

2 Swirl Burner and Flame Conditions

A schematic diagram of the experimental burner is given in Figure 1. The burner has a fuel jet of diameter 3.6 mm surrounded by a bluff body of D=50 mm diameter. The burner also has a primary annulus with 5 mm wide around the bluff body which provides both axial and swirling air. Swirl is introduced aerodynamically by using tangential ports 300 mm upstream of the burner exit. The burner is installed in a wind tunnel which provides a co-flow secondary air stream. In our computations we assumed $x\,mm$ as axial distance and $r\,mm$ as radial distance.

The swirl number S is usually defined as the ratio between axial flux of the angular momentum to the axial flux of axial momentum such that:

$$S = \frac{\int_0^R \rho <U> <W> r^2 dr}{R \int_0^R \rho <U>^2 r dr} \tag{1}$$

Where $<U>$ and $<W>$ are the mean axial and tangential velocities at the exit plane, ρ is the density and R is a characteristic length. However, the present burner considered the geometric swirl number S_g , which is defined as the ratio between bulk tangential to bulk axial velocity and found that the geometric swirl number $S_g$is linearly proportional to actual swirl number S [1]. The Reynolds numbers for the fuel jet and primary annulus is defined as $Re_j = U_j \times d_j/\nu$ and $Re_s = U_s \times r_s/\nu$, where d_j is the diameter of the fuel

Table 1: Parameters of the investigated cases

Case	Fuel *(vol.)*	f_s	U_e m/s	U_s m/s	W_s m/s	U_{jet} m/s	Re_{jet}	Re_s	S_g
SM1	CH_4	0.05	20	38.2	19.1	32.7	7,200	75,900	0.50
SM1a	CH_4	0.05	20	38.2	29.3	32.7	7,200	75,900	0.75
SM1b	CH_4	0.05	20	38.2	39.0	32.7	7,200	75,900	1.0

inlet, U_j is the bulk jet velocity, U_s is the annulus bulk axial velocity and r_s is the outer radius of the annulus [1]. The experimental velocity variables were the fuel jet velocity U_j, the bulk axial and tangential velocities U_s and W_s of the primary air stream, and the mean co-flow velocity U_e of the secondary air stream.

In the present study only pure methane SM1 flame from the experimental data base [1, 23, 34] is considered which has a fuel jet velocity of 32.7 m/s with a swirl number $S = 0.5$. The flame contains two recirculation zones, the first closer to the bluff body which stagnates at about 43 mm and the second further downstream which stagnates at 70 mm on the centreline. The mean stoichiometric mixture fraction occurs on the centreline at an axial position that is consistent with the visible length of the flame (0.12 m) [34]. In addition to SM1 flame, two more numerical flames have been considered and defined as SM1a and SM1b with corresponding swirl numbers 0.75 and 1.0 respectively. The table shows the considered parameters for the three cases.

3 Governing Equations and Modelling

The LES calculation consists of solving the temporal development of large scale structures by applying spatial filter to the governing equations. In this work, we consider implicit box (top-hat) filter, which naturally fit into the finite volume formulation. By applying a spatial filter, the filtered governing equations for mass, momentum and mixture fraction can be written as follows:

$$\frac{\partial \overline{\rho}}{\partial t} + \frac{\partial}{\partial x_j}\overline{\rho}\widetilde{u_i} = 0 \tag{2}$$

$$\begin{aligned} \frac{\partial}{\partial t}(\overline{\rho}\widetilde{u_i}) + \frac{\partial}{\partial x_j}(\overline{\rho}\widetilde{u_i}\widetilde{u_j}) = -\frac{\partial \overline{p}}{\partial x_i} &+ \frac{\partial}{\partial x_j}\left(2\overline{\rho}(\nu+\nu_t)\left[\widetilde{S}_{ij} - \frac{1}{3}\delta_{ij}\widetilde{S}_{kk}\right]\right) \\ &+ \frac{1}{3}\frac{\partial}{\partial x_j}[\overline{\rho}\delta_{ij}\tau_{kk}] + \overline{\rho}g_i \\ \text{with the strain rate} \quad \widetilde{S}_{ij} &= \frac{1}{2}\left(\frac{\partial \widetilde{u_i}}{\partial x_j} + \frac{\partial \widetilde{u_j}}{\partial x_i}\right) \end{aligned} \tag{3}$$

$$\frac{\partial}{\partial t}(\overline{\rho}\widetilde{f}) + \frac{\partial}{\partial x_j}(\overline{\rho}\widetilde{f}\widetilde{u_j}) = \frac{\partial}{\partial x_j}\left(\overline{\rho}\left[\frac{\nu}{\sigma} + \frac{\nu_t}{\sigma_t}\right]\frac{\partial \widetilde{f}}{\partial x_j}\right) \tag{4}$$

Where, ρ is the density, u_i is the velocity component in the x_i direction, ν and ν_t are the laminar and turbulent viscosity, p is the pressure, g_i is the gravitational acceleration, f is the mixture fraction and τ_{kk} is the isotropic part of the sub-grid scale tensor. The laminar and turbulent Schmidt numbers σ and σ_t were set to 0.7 and 0.4 respectively [39].

For unclosed terms in the momentum and the mixture fraction equations, the sub-grid scale contribution is modelled via turbulent eddy viscosity ν_t by applying a Smagorinsky [42] eddy viscosity model.

$$\nu_t = C_s\Delta^2\left|S_{ij}\right| = C_s\Delta^2\left|\frac{1}{2}\left(\frac{\partial \widetilde{u_i}}{\partial x_j} + \frac{\partial \widetilde{u_j}}{\partial x_i}\right)\right| \tag{5}$$

Where C_s is the model parameter, Δ is the filter width and S_{ij} is the strain rate tensor. The isotropic part of the stress tensor included into the pressure correction equation such that $\overline{P} = \overline{p} - \frac{1}{3}\tau_{kk}$. The Smagorinsky model parameter C_s is dynamically calculated using the localised dynamic procedure of Piomelli & Liu [37]. Since the chemical reactions occur

in sub-grid scale, modelling is required for the combustion. In this work we used the mixture fraction based approach with an assumed beta pdf. A steady laminar flamelet is used as a combustion model and thermo-chemical variables such as density, temperature are evaluated using Favre filtered mixture fraction, mixture fraction variance and scalar dissipation rate. The gradient transport model is used for the calculation of mixture fraction variance. The flamelets were generated using Flamemaster code [38] with the incorporation of detailed chemistry mechanism, GRI 2.11 [5].

4 Numerical Computation

The resultant governing equations and boundary conditions are numerically solved by means of a pressure based finite volume methodology on Cartesian coordinate system. All simulations were performed using the LES code PUFFIN originally developed by Kirkpatrick et al. [27] and later extended by Ranga Dinesh [12, 13]. Second order central differences (CDS) are used for the spatial discretisation of all terms in both the momentum equation and the pressure correction equation. This minimises the projection error and ensures convergence in conjunction with an iterative solver. The diffusion terms of the mixture fraction transport equation are also discretised using the second order CDS. However, the convection term in the mixture fraction transport equation is discretised using a Simple High Accuracy Resolution Program (SHARP) developed by Leonard [30]. The time derivative of the mixture fraction is approximated using the Crank-Nicolson scheme. The momentum equations are integrated in time using a second order hybrid scheme. Advection terms are calculated explicitly using second order Adams-Bashforth while diffusion terms are calculated implicitly using second order Adams-Moulton to yield an approximate solution for the velocity field and finally the mass conservation is enforced through a pressure correction step. Several outer iterations (8-10) are used to achieve the convergence for each time step and time steps are advanced with variable Courant number in the range of 0.3-0.6. The Bi-Conjugate Gradient Sta-

bilized (BiCGStab) method with a Modified Strongly Implicit (MSI) preconditioner is used to solve the system of algebraic equations resulting from the discretisation.

All three simulations for flames SM1, SM1a and SM1b were performed on Cartesian grids with the dimension of $300 \times 300 \times 250$ mm in x,y and z directions by employing 3.4 million cells. The inlet mean velocity profiles are generated from the power law such that

$$<U>= C_0 U_j \left(1 - \frac{r}{1.01 \cdot r_j}\right)^{1/7} \tag{6}$$

Where U_j is the bulk velocity, r is the radial distance from the jet centre line and r_j is the fuel jet radius of 1.8 mm. The scale 1.01 is introduced to ensure that velocity gradients are finite at the walls. Similar format is used for the primary annulus with U_j replaced by bulk axial velocity U_s and bulk swirling velocity W_j and r being the radial distance from the centre of the primary annulus.

The velocity fluctuations for both axial and swirl components are generated from a Gaussian random number generator and added them to the mean velocity profiles. A top hat profile is used as the inflow condition for the mixture fraction. A free slip boundary conditions is applied at the solid walls and at the outflow place, a convective boundary condition is used for the velocities and a zero normal gradient is used for the mixture fraction. Simulations were performed for a sufficient time to achieve convergence before store data for the intermittency calculation.

5 Results and Discussion

This section presents a detailed description of the computed pdf distributions and radial variation of intermittency fields for the velocity, mixture fraction and temperature for three different flames. The considered flames were SM1, SM1a and SM1b with swirl

numbers 0.5, 0.75 and 1.0 respectively. The intention is to study the effects of swirl on turbulent intermittency and scalar mixing in the presence of precession, recirculation and vortex breakdown. Our earlier LES investigations on SM1 flame found good qualitative comparisons for velocity and scalar fields with experimental measurements [33] by capturing the bluff body stabilised recirculation zone, the downstream VB bubble and also investigated the centre jet precession and PVC structures along with power spectra analysis [14]. Therefore, the present work continues the previous investigations to study the influence of swirl on turbulent intermittency aiming for further improvement of tackling combustion intermittency such as the characteristics of scalar dissipation rate and unsteady strain in turbulent non-premixed combustion with complex flow conditions.

Various methods are available to determine the intermittency factor (γ) in a heated flow for variables such as velocity, passive and active scalars [3, 47]. The following section provides a brief discussion of the intermittency calculation procedure used in this work. The most common method is to estimate a pdf by computing a normalised histogram. This method assumes that the pdf is smooth at the scale of one histogram bin. By applying this procedure, the pdfs were calculated from no less than 4000 measurements at each spatial location using 50 bins equally spaced over the $3-\sigma$ limits of the data. The distributions are normalised hence

$$\int_0^1 P(f)\, df = 1 \tag{7}$$

Therefore the intermittency for velocity, mixture fraction and temperature can be defined as the fraction of time that the variable value is greater than an arbitrary threshold value. The corresponding intermittency is calculated from the probability density distribution of the instantaneous values. For example if select a threshold value of f_{th} for variable f, the area under the probability density distribution relates to the intermittency such that:

$$\gamma = P(f > f_t h) \tag{8}$$

Figures 2-4 show snapshots of the flame temperature for SM1, SM1a and SM1b respectively. All three flames show high temperature regions on the boundary of the first bluff body stabilised recirculation zone and further downstream near the centreline region inside the second downstream recirculation zone. The small neck region is visible for SM1 flame near x=60 mm (downstream from the burner exit plane) which has also been observed by the experimental data [23]. Moreover, all three flames show stagnation regions in the upstream first recirculation zone where the mean axial velocity is zero just above 40 mm and for the downstream second recirculation zone where the axial velocity on the centreline is below zero around x=70-130 mm depend on the strength of the swirl. Therefore this work focuses on four important axial positions to produce pdf and radial variation of intermittency for velocity, mixture fraction and temperature. The first axial location selected inside the bluff body stabilised recirculation zone (x=30 mm), the second location situated between upstream and downstream recirculation zones (x=55 mm), the third axial location is inside the downstream recirculation zone (x=100 mm) and the fourth axial location further downstream and on the boundary of the downstream recirculation zone (x=155 mm). The selected axial locations are marked in each figure. The pdfs for velocity, mixture fraction and temperature at each axial locations (x=30, 55, 100, 155 mm) are generated for equal radial distances (r=0, 12, 24, 32 mm).

5.1 Velocity Intermittency

Figures 5-8 show the pdf of axial velocity at x=30, 55, 100 and 155 mm respectively. The pdfs of velocity for all three swirl numbers show similar variation for many radial locations at both axial locations. As seen in Fig. 5, the pdf at x=30 mm show similar variation for all three cases at r=0, 12 mm, but start to deviate at far radial locations (r=24, 32 mm) due to high centrifugal forces at the higher swirl number. The pdfs of

velocity at x=55 mm (Fig. 6) again show similar variation near the centreline and start to deviate at far radial locations. However as seen in both Figs. 7 and 8, the results show similar variation even at far radial locations. It is important to note that both LES and experimental results observed that the centre jet has an irregular random motion and the large scale wobbling motion of the jet tip for flame SM1 [14]. Since the centre jet axially extentds closer to x=30 mm, the pdfs of velocity on the centreline at x=30 mm show a non-Gaussian behaviour (r=0 mm) due to direct impact of wobbling motion of the centre jet tip. However, all figures at remaining axial locations (x=55, 100, 155 mm) show that the pdfs near the centreline follow the Gaussian shape and then move to a delta function at far radial locations. Moreover, close to the centre-line (r=0, 12 mm) these distributions are relatively broad and generally Gaussian, whereas with increasing radial distance they narrow and ultimately form spikes on the co-flow velocity (r=32 mm). The pdfs of velocity also show more rapid decay in the axial velocity with increasing radial distance (Figs. 5-8). This can be expected as the axial variation of both the upstream and downstream recirculation zones vary with respect to swirl number. The pdfs of velocity further indicate that the coupling between turbulence and heat release in the presence of precession and recirculation could form different intermittent regimes closer to the centreline contrast to the turbulent jet flame where intermittency can expect near the outer region.

Figure 9 shows the radial profiles of velocity intermittency at x=30, 55, 100 and 155 mm respectively. Since the burner has a secondary co-flow velocity of 20 m/s, the calculation used a threshold value of $u_{th} = 10\,m/s$ (half of the secondary axial co-flow velocity). The variation of the intermittency values indicate the effect of swirl on turbulent to non-turbulent phenomena with respect to a given threshold value. As expected, differences of the velocity intermittency appears mainly near the centreline region. For example, Fig. 9 shows little effect of swirl on the velocity intermittency near the centreline inside the bluff body stabilised recirculation zone (x=30mm). However, the effect of swirl on velocity intermittency is apparent at the other axial locations such as between two recirculation

regions (x=55 mm), inside the second recirculation region (x=100 mm) and downstream boundary of the second recirculation region (x=155 mm). The effect of swirl on velocity intermittency also indicates the phenomena of small scale turbulent fluctuation which is an important issue for the temperature intermittency. However, the radial profiles of velocity intermittency follows a similar shape distribution at far radial positions at all considered axial locations. This can be expected due to co-flow velocity of 20 m/s which is twice as a considered threshold value (10 m/s) for deriving velocity intermittency.

5.2 Mixture Fraction Intermittency

In Figs. 10-13 the pdfs of the mixture fraction is displayed at axial locations x=30, 50, 100 and 150 mm respectively. These results are qualitatively similar to those derived from the velocity pdfs. The centreline mixture fraction pdfs at x=30 mm (Fig. 10) show non-Gaussian behaviour due to the centre jet precession and thus indicate important characteristics of mixing compared to the standard Gaussian behaviour of a turbulent jet diffusion flame. However, as expected the centreline non-Gaussian is gradually converted to Gaussian at far downstream axial locations (Figs. 11, 12, Figs. 13). The mixture fraction pdfs plots indicate that the high swirl (S=1.0) indicates more mixing even at far radial locations (r=24, 32 mm) for all selected axial positions. The Gaussian shapes of pdfs eventually fall into delta function at far radial axial locations.

Figure 14 shows the radial profiles of intermittency at x=30, 55, 100 and 155 mm respectively. The present study used a threshold value of $f_{th} = 0.054$ with a stoichiometric mixture fraction for pure methane SM1 swirling flame [23, 34]. The intermittency values follow Gaussian shape at all axial locations. The effect of swirl on mixture fraction intermittency is minimum at first three axial locations for the selected threshold value. However, as seen in Fig. 14 the swirl starts to affect the mixture fraction intermittency at far downstream axial location (x=155 mm) due to lower turbulence for low swirl case (S=0.5) and the turbulence is gradually improved for increased swirl numbers (S=0.75,

1.0)

5.3 Temperature Intermittency

The pdfs of temperature at x=30, 55, 100 and 155mm are shown in Figs. 15-18. Although the time averaged mean temperature field for SM1 flame shows good agreement with the experimental data [33], the instantaneous pdfs of temperature values show interesting variation from the centreline to far radial locations and thus indicate a sign of temperature intermittency for certain regions of the flame. Again, similar to velocity and mixture fraction the temperature field follows the non-Gaussian shape on the centreline at x=30 mm (Fig. 15). However, at x=55 mm the pdf of temperature follows a Gaussian shape on the centreline and then changing to a delta function at far radial locations. The effect of swirl is also apparent at far radial locations as temperature pdf shows an intermediate shape between Gaussian and delta function at both r=24 mm and 32 mm for high swirl number (S=1.0). It is also important to note that the small variation of mixture fraction could lead to a variation of temperature as a result of using the steady laminar flamelet model. Therefore the pdf variation of mixture fraction is directly linked to the pdf of temperature and thus form a non-Gaussian shape. Additionally the increase in swirl number has an effect on flame temperature in a region close to the centreline (r=0 mm and 12 mm) and also at far radial locations (r=24 mm). The variation of the temperature pdfs at intermediate radial locations between two recirculation zones and inside a vortex breakdown bubble (Figs. 17, 18) may be subjected to high shear effects and rapid variation of the turbulence intensities, which forms a different shape between the Gaussian distribution and the delta function.

Figure 19 shows the radial variation of intermittency for temperature at x=30, 55, 100 and 150 mm respectively. Here we have used a threshold value of $t_h = 750\,k$ which is approximately half the value of the maximum mean temperature calculated from the simulation. As seen in Fig. 19, the centreline intermittency values show less than unity

and thus indicate a sort of reduced temperature with respect to a threshold value for all three cases. This has been observed inside the upstream recirculation zone where turbulence can play a vital role with the presence of counter rotating vortices. The temperature intermittency at the axial location x=55 mm shows non-smoothness for all three flames at particular radial locations where rapid changes of the velocity fluctuations occur. This resulted from the mixture fraction variance which linked to rapid velocity fluctuations in the region between two recirculation zones.

In summary the swirling flames considered for the intermittency investigations having complex flow structures where there are two recirculation zones (bluff body stabilised and swirl induced), collar-like flow structure and also centre jet precession behaviour. Therefore, these flames exhibit a number of high shear layers and important flow regimes where the coupling of swirl-turbulent-chemistry plays an important role and here we have discussed the intermittent nature of turbulent swirling flames using localised dynamic LES subgrid turbulence model and steady laminar flamelet combustion model. However, using a steady laminar flamelet model might restrict the combustion physics of intermittent behaviour especially for the temperature field and more advanced flamelet based models such as, unsteady flamelet model, flamelet progress variable approach may be promising to identify intermittency of the scalar dissipation rate (unsteady strains) and thus temperature of complex swirling flames.

6 Conclusions

A large eddy simulation has been applied to study the effect of swirl on intermittency of turbulent non-premixed flames. Probability density functions and intermittency profiles have been generated for velocity, mixture fraction and temperature. Derived probability density functions show changes from Gaussian shape to delta function with increased radial distance at several selected axial locations. However, non-Gaussian behaviour pdf is also observed on the centreline in a region where centre jet precession occurs. The vari-

ation from turbulent to non-turbulent phenomena for a given threshold value is always predicted to be more rapid for the velocity due to the formation of recirculation zones. The differences of the intermittency in velocity and scalars for a complex swirling flame in the presence of one or more recirculation zones and precession motion demonstrate the uncertainties in turbulent/non-turbulent phenomena and its direct effect on chemical reaction and heat release. Therefore more investigations should be carried out to outline relations between intermittency and the rate of turbulent and molecular mixing rates for complex and practically relevant turbulent swirling flames.

Acknowledgements

This work was supported by the Engineering and Physical Research Council (EPSRC) under grant number (EP/E036945/1) on the Modelling and Simulation of Intermittent Flows.

References

[1] Y. M. Al-Abdeli and A. R. Masri. Stability characteristics and flowfields of turbulent non-premixed swirling flames. *Combust. Theory Model.*, 7:731–766, 2003.

[2] P. A.Libby. On the prediction of intermittent turbulent flows. *J. Fluid. Mech.*, 68:273–279, 1975.

[3] R. W. Bilger, R. A. Antonia, and K. R. Sreenivasan. Determination of intermittency from the probability density function of a passive scalar. *Phys. Fluids*, 19:1471–1474, 1976.

[4] G. L. Boudier, Y. M. Gicquel, and T. J. Poinsot. Effects of mesh resolution on large eddy simulations of reacting flows in complex geometries. *Combust. Flame*, 155:196–214, 2008.

[5] C.T. Bowman, R.K. Hanson, D.F. Davidson, W.C. Gardiner Jr., V. Lissianski, G.P. Smith, D.M. Golden, M. Frenklach, and M. Goldenberg. Gri 2.11. *http://www.me.berkeley.edu/gri_mech, 11/05/2007*, 2006.

[6] S. Byggstoyl and W. Kollmann. Closure model for intermittent turbulent flows. *Int. J. Heat Mass Transfer*, 24:1811–1818, 1981.

[7] R. Chevray and N. K. Tutu. Intermittency and preferential tranpsort of heat in a round jet. *J. Fluid. Mech.*, 88:133–145, 1978.

[8] J. R. Cho and M. K. Chung. A k-epsilon-gamma equation turbulence model. *J. Fluid Mech.*, 237:301–322, 1992.

[9] S. Corrsin and A. L. Kistler. Free stream boundaries of turbulent flows. *NACA Report*, 1244, 1955.

[10] A. Dewan, J. H. Arakeri, and J. Srinivasan. A new turbulence model for the axisymmetric plane. *J. Appl. Math Model.*, 21:709–719, 1997.

[11] F. DiMare, W. Jones, and K. Menzies. Large eddy simulation of a model gas turbine combustor. *Combust. Flame*, 137:278–294, 2004.

[12] K. K. J. Ranga Dinesh. *Large eddy simulation of turbulent swirling flames*. PhD thesis, Loughborough University, UK, 2007.

[13] K. K. J. Ranga Dinesh, K. W. Jenkins, M. P. Kirkpatrick, and W. Malalasekera. Identification and analysis of instability in non-premixed swirling flames using les. *Combust. Theo. Model.*, 13:947–971, 2009.

[14] K. K. J. Ranga Dinesh, K. W. Jenkins, M. P. Kirkpatrick, and W. Malalasekera. Modelling of instabilities in swirling flames. *J. Fuel*, 89:10–18, 2010.

[15] C. Dopazo. On conditioned averages for intermittent turbulent flows. *J. Fluid. Mech.*, 81:433–445, 1977.

[16] M. P. Escudier and J. J. Keller. Recirculation in swirling flows: a manifestation of vortex breakdown. *AIAA J.*, 23:111–116, 1985.

[17] J. D. Gibbson and C. R. Doering. Intermittency in solutions of the three dimensional navier-stokes equations. *J. Fluid Mech.*, 478:227–235, 2003.

[18] F. F. Grinstein and C. Fureby. Les studies of the flow in a swirl gas combustor. *Proc. Combust. Inst.*, 30:1791–1798, 2005.

[19] A. K. Gupta, D. G. Lilly, and N. Syred. Swirl flows. In *Swirl flows*. Kent Engl: Abacus, 1984.

[20] Y. Huang, H. G. Sung, S. Y. Hsieh, and V. Yang. Large eddy simulation of combustion dynamics of lean premixed swirl stabilised combustor. *J. Prop. Power*, 19:782–794, 2003.

[21] J. Jimenez. Intermittency and cascades. *J. Fluid Mech.*, 409:99–120, 2000.

[22] K. Kalita, A. Dewan, and A. K. Dass. Computation of the turbulent plane plume using the model. *J. Appl. Math Model.*, 24:815–826, 2000.

[23] P. A. M. Kalt, Y. M. Al-Abdeli, A. R. Masri, and R. S. Barlow. Swirling turbulent non-premixed flames of methane: Flowfield and compositional structure. *Proc. Combust. Inst.*, 29:1913–1919, 2002.

[24] A. Kempf, W. Malalasekera, K. K. J. Ranga Dinesh, and O. Stein. Large eddy simulations of swirling non-premixed flames with flamelet models:a comparison of numerical methods. *Flow Turb. Combust.*, 81:523–561, 2008.

[25] A. R. Kerstein. Turbulence in combustion process: Modelling and challenges. *Proc. Combust. Inst.*, 29:1763–1773, 2002.

[26] W. W. Kim and S. Syed. Large eddy simulation needs for gas turbine combustor design. *AIAA*, pages 2004–0331, 2004.

[27] M. P. Kirkpatrick, S. W. Armfield, and J. H. Kent. A representation of curver boundaries for the solution of the navier-stokes equations on a staggered three dimensional cartesian grid. *J. Comput. Phys.*, 184:1–36, 2003.

[28] P. S. Klebanoff. Characteristics of turbulence in boundary layer with zero pressure gradient. *NACA Report*, 1247, 1955.

[29] W. Kollamann and J. Janicka. The probability function of a passive scalar in turbulent shear flows. *Phy. Fluids*, 25:1755–1769, 1982.

[30] B. P. Leonard. Sharp simulation of discontinuities in highly convective steady flow. Technical Report 100240, NASA Tech. Mem., 1987.

[31] O. Lucca-Negro and T. O'Doherty. Vortex breakdown: a review. *Prog. Energy Combust. Sci.*, 27:431–481, 2001.

[32] K. Mahesh, G. Constantinescu, G. Iaccarino S. Apte, F. Ham, and P. Moin. Large eddy simulation of reacting turbulent flows in complex geometries. *ASME J.Appl. Mech.*, 73:374–381, 2006.

[33] W. Malalasekera, K. K. J. Ranga Dinesh, S. S. Ibrahim, and A. R. Masri. Les of recirculation and vortex breakdown in swirling flames. *Combust. Sci. Tech.*, 180:809–832, 2010.

[34] A. R. Masri, P. A. M. Kalt, and R. S. Barlow. The compositional structure of swirl stabilised turbulent non-premixed flames. *Combust.Flame*, 137:1–37, 2004.

[35] I. Nakamura, Y. Sakai, and H. Tsunoda. On conditional statistics of the diffusion field of matter by a point source plume in uniform mean shear flow. *JSME Int. J.*, 32:180–190, 1989.

[36] C. D. Pierce and P. Moin. Progress-variable approach for large eddy simulation of non-premixed turbulent combustion. *J. Fluid Mech.*, 504:73–97, 2004.

[37] U. Piomelli and J. Liu. Large eddy simulation of rotating channel flows using a localized dynamic model. *Phys. Fluids*, 7:839–848, 1995.

[38] H. Pitsch. A C++ computer program for 0-d and 1-d laminar flame calculaions. Technical report, RWTH Aachen, 1998.

[39] H. Pitsch and H. Steiner. Large eddy simulation of a turbulent piloted methane-air diffusion flame(sandia flame d). *Phys. Fluids*, 12(10):2541–2554, 2000.

[40] S. B. Pope. Calculation of plane turbulent jet. *AIAA J.*, 22:896–904, 1984.

[41] L. Selle, G. Lartigue, T. Poinsot, and R. Koch et al. Compressible large eddy simulation of turbulent combustion in complex geometry on unstructured meshes. *Combust. Flame*, 137:489–505, 2004.

[42] J. Smagorinsky. General circulation experiments with the primitive equations, the basic experiment. *Mon. Weath. Rev.*, 91:99–164, 1963.

[43] K. R. Sreenivasan. On the fine scale intermittency of turbulence. *J. Fluid Mech.*, 151:81–103, 1985.

[44] N. Syred. A review of instability and oscillation mechanisms in swirl combustion systems. *Prog. Energy Combust. Sci.*, 32:93–161, 2006.

[45] N. Syred and J. M. Beer. Combustion in swirling flows: a review. *Combust. Flame*, 23:143–201, 1974.

[46] A. A. Townsend. Local isotropy in the turbulent wake of cylinder. *Austr. J. Sci. Res.*, 1:161–168, 1948.

[47] R. W.Schefer and R. W.Dibble. Mixture fraction field in a turbulent non-reacting propane jet. *AIAA J.*, 39:64–72, 2001.

[48] I. Wygnanski and H. E. Fiedler. Some measurements in the self preserving jet. *J. Fluid. Mech.*, 38:577–612, 1969.

[49] Li Y and C. Meneveau. Intermittency trends and lagrangian evolution of non-gaussian statistics in turbulent flow and scalar transport. *J. Fluid Mech.*, 558:133–142, 2006.

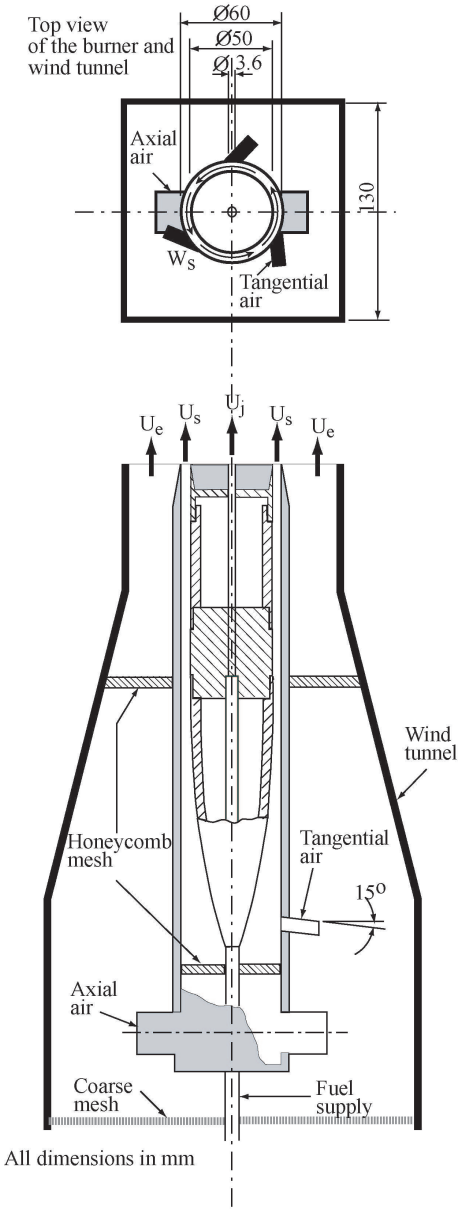

Figure 1: Schematic of the swirl burner

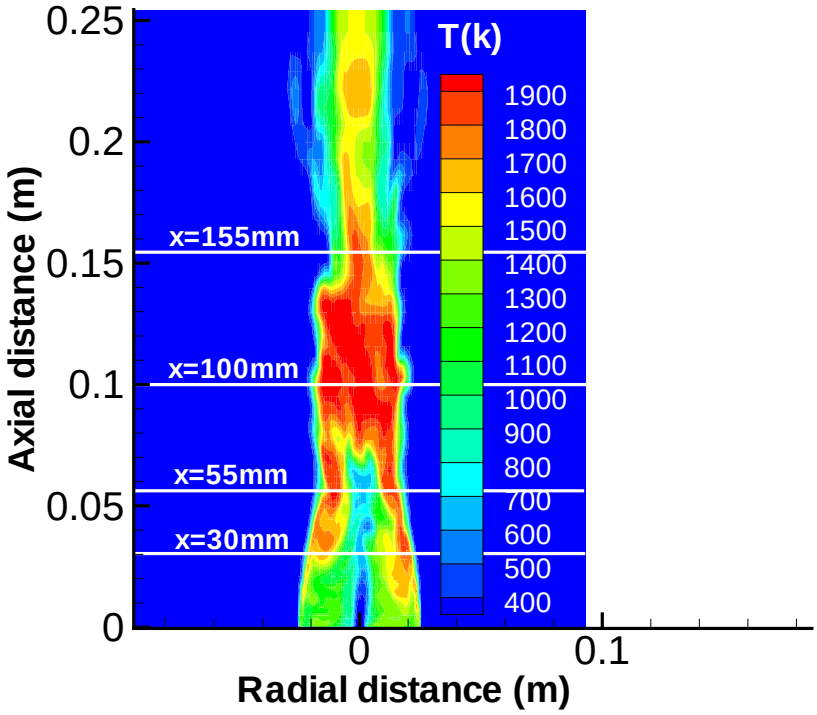

Figure 2: Snapshot of SM1 flame temperature

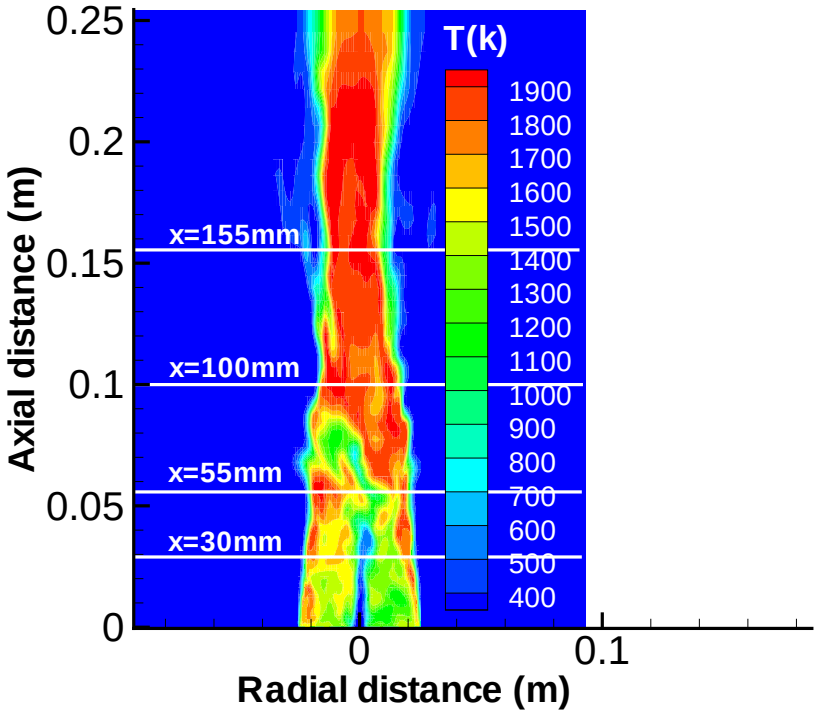

Figure 3: Snapshot of SM1a flame temperature

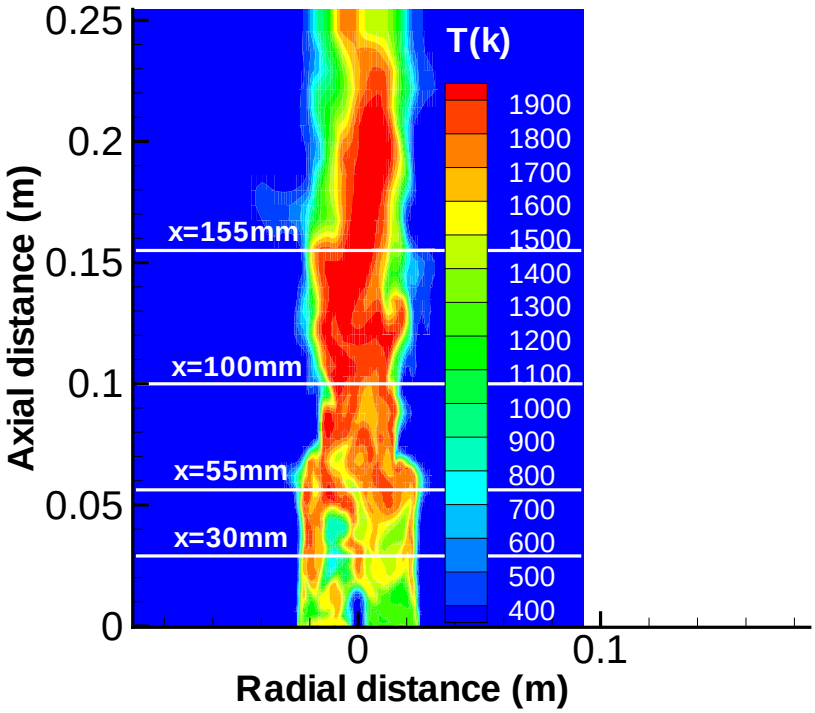

Figure 4: Snapshot of SM1b flame temperature

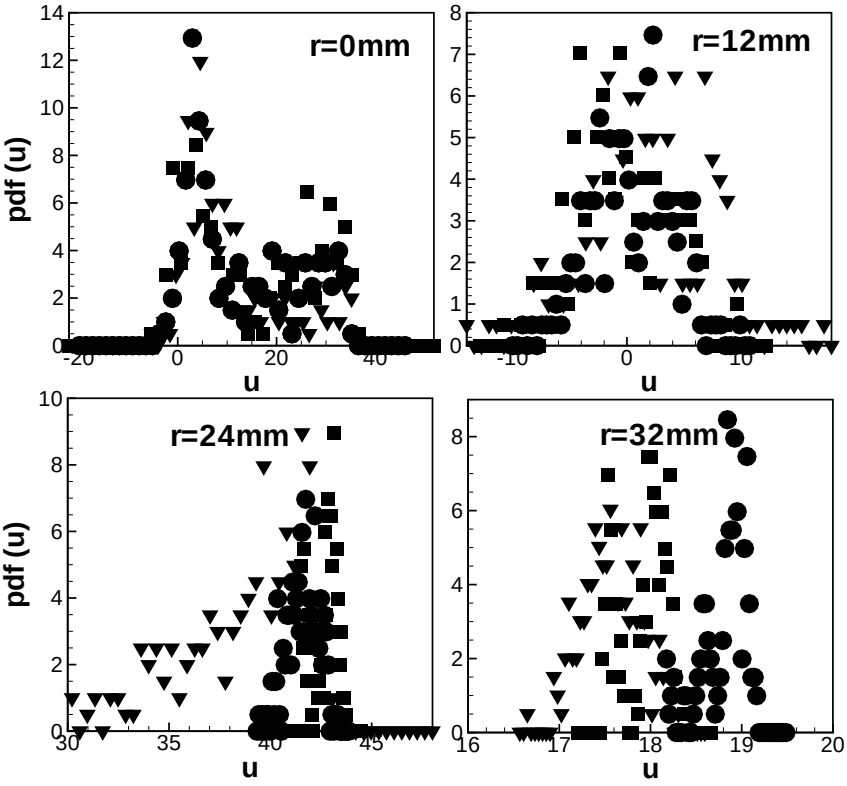

Figure 5: Comparisons of velocity pdfs at x=30mm at equidistant radial locations (a), (b), (c) and (d). Here circles, squares and inverted triangles denote results for swirl numbers 0.5, 0.75 and 1.0

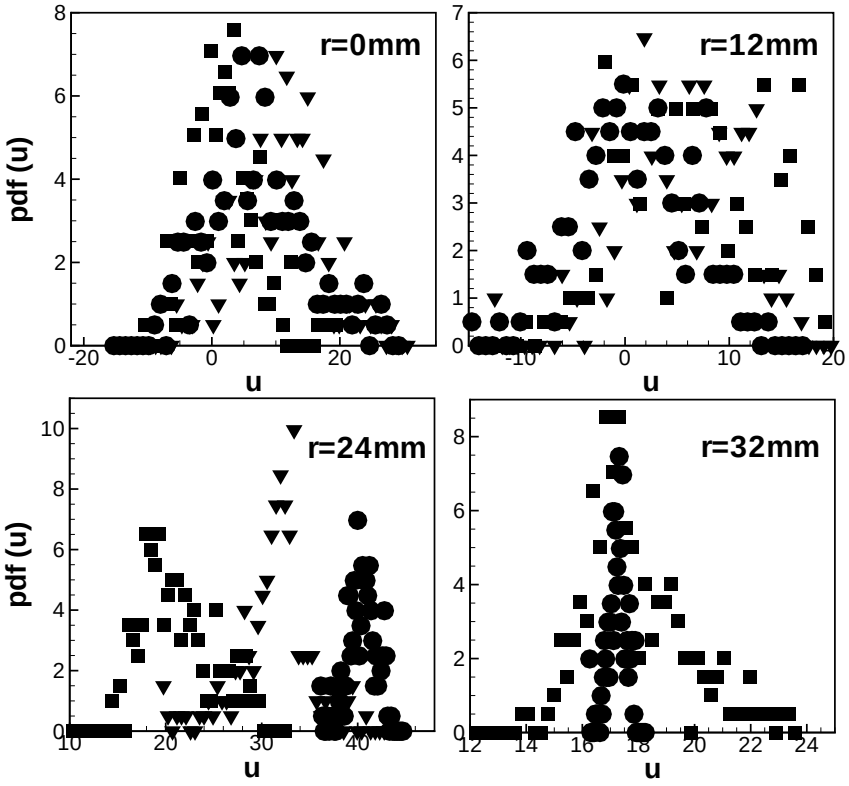

Figure 6: Comparisons of velocity pdfs at x=55mm at equidistant radial locations (a), (b), (c) and (d). Here circles, squares and inverted triangles denote results for swirl numbers 0.5, 0.75 and 1.0

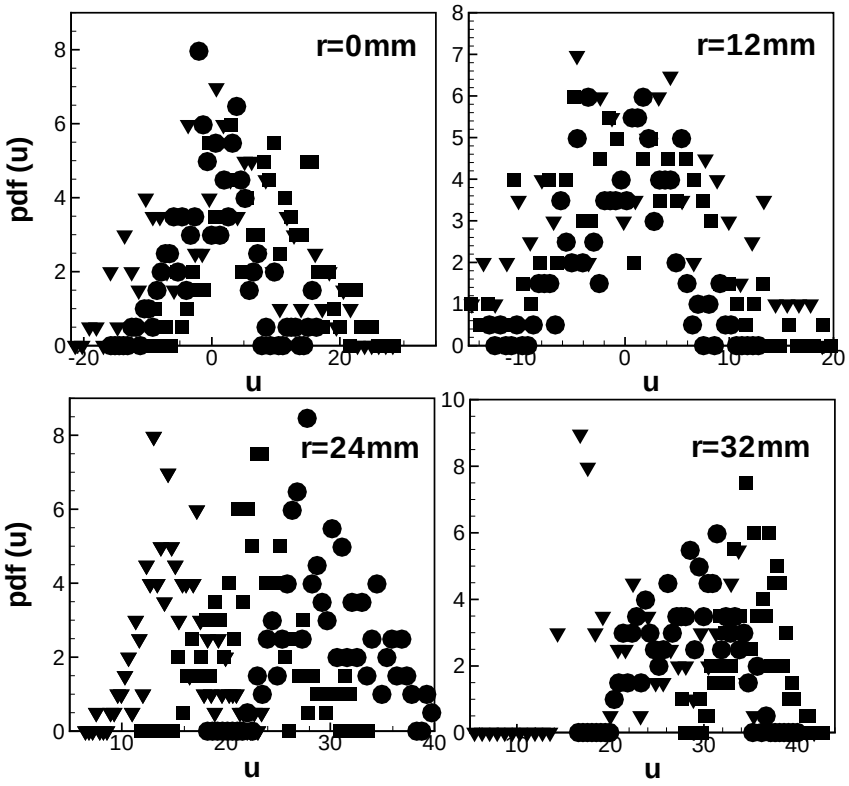

Figure 7: Comparisons of velocity pdfs at x=100mm at equidistant radial locations (a), (b), (c) and (d). Here circles, squares and inverted triangles denote results for swirl numbers 0.5, 0.75 and 1.0

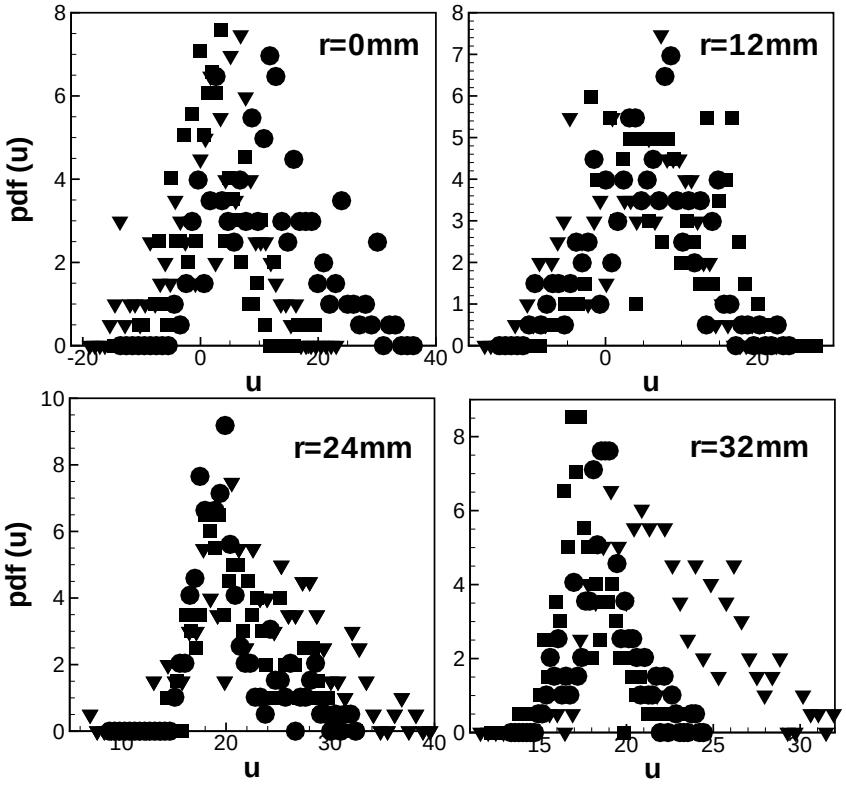

Figure 8: Comparisons of velocity pdfs at x=155mm at equidistant radial locations (a), (b), (c) and (d). Here circles, squares and inverted triangles denote results for swirl numbers 0.5, 0.75 and 1.0

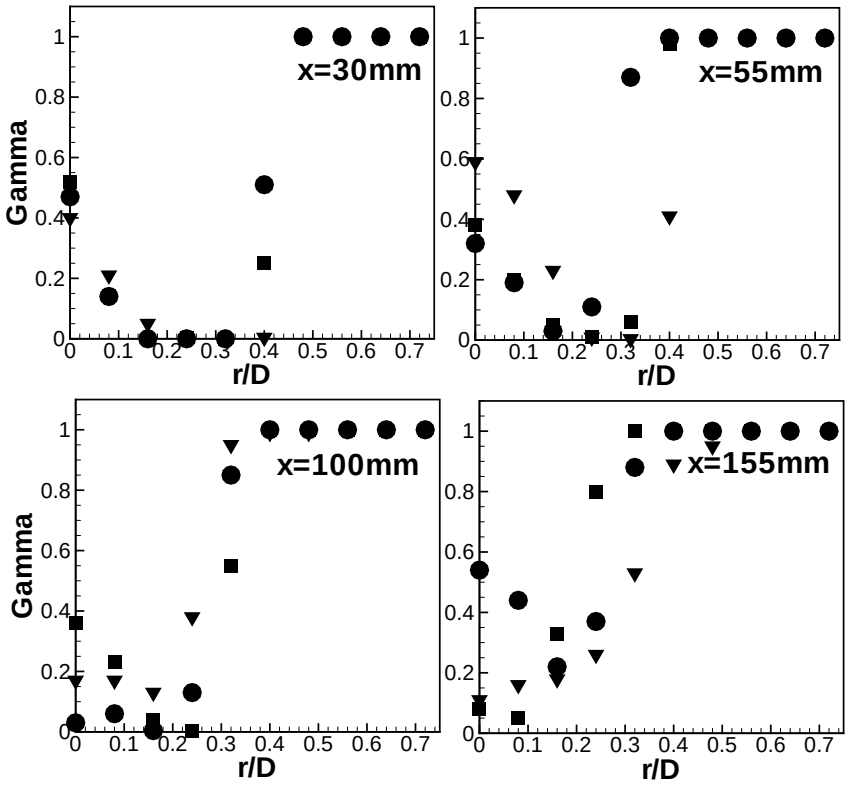

Figure 9: Radial profiles of velocity intermittency at (a) x=30mm, (b) x=55mm, (c) x=100mm and (d) x=155mm. Here circles, squares and inverted triangles denote results for swirl numbers 0.5, 0.75 and 1.0

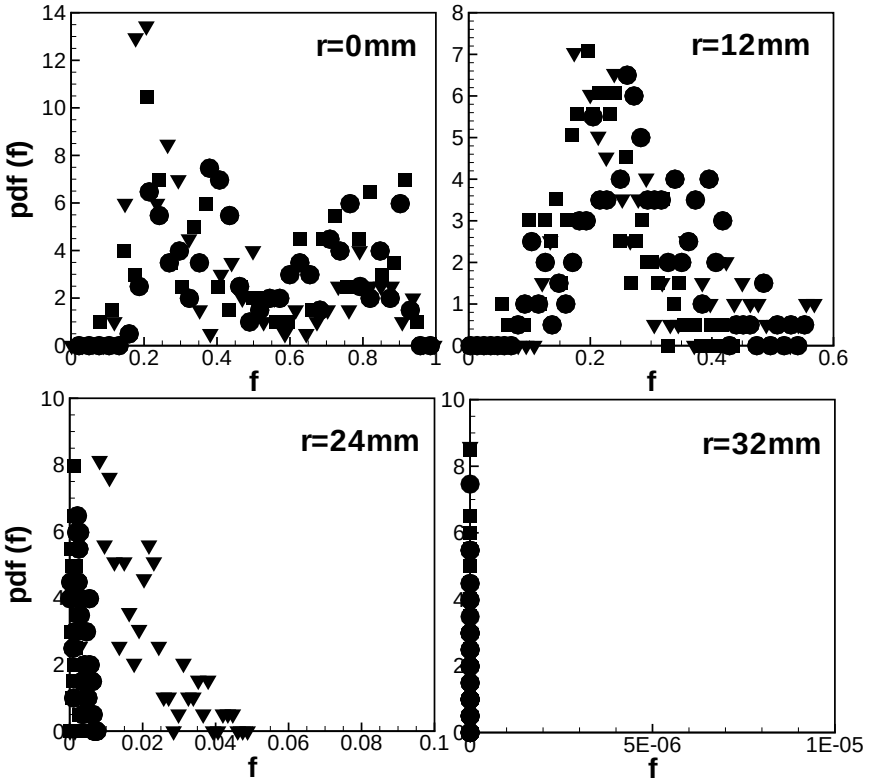

Figure 10: Comparisons of mixture fraction pdfs at x=30mm at equidistant radial locations (a), (b), (c) and (d). Here circles, squares and inverted triangles denote results for swirl numbers 0.5, 0.75 and 1.0

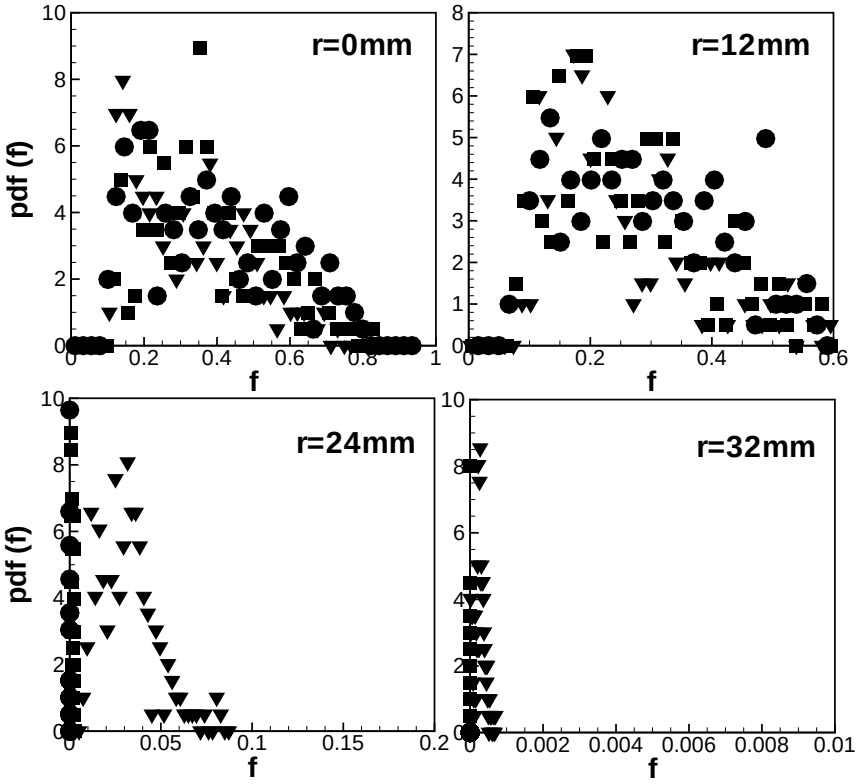

Figure 11: Comparisons of mixture fraction pdfs at x=55mm at equidistant radial locations (a), (b), (c) and (d). Here circles, squares and inverted triangles denote results for swirl numbers 0.5, 0.75 and 1.0

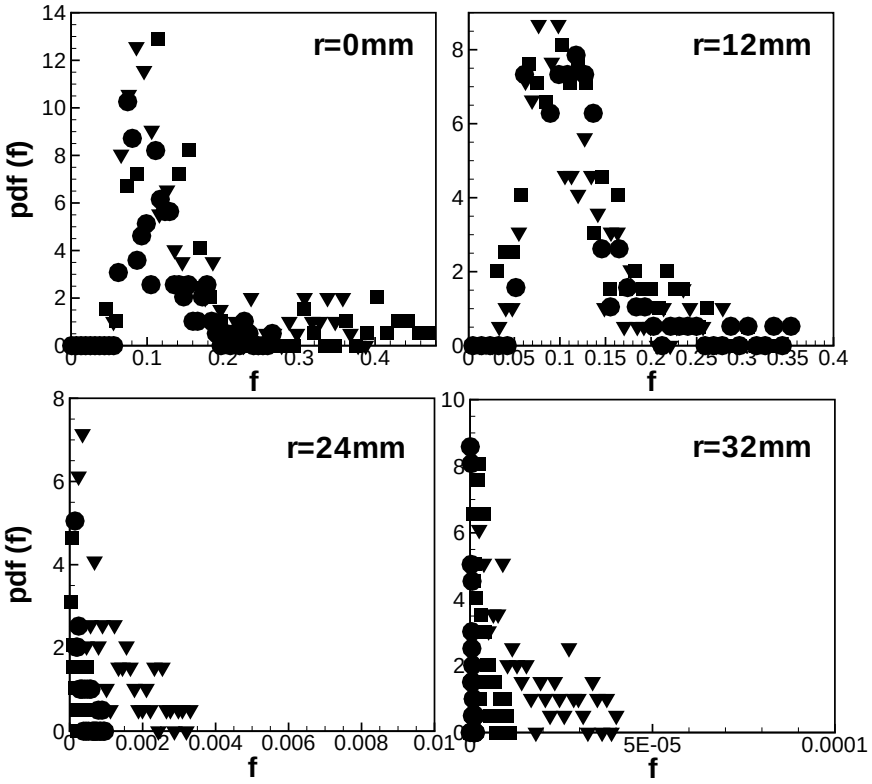

Figure 12: Comparisons of mixture fraction pdfs at x=100mm at equidistant radial locations (a), (b), (c) and (d). Here circles, squares and inverted triangles denote results for swirl numbers 0.5, 0.75 and 1.0

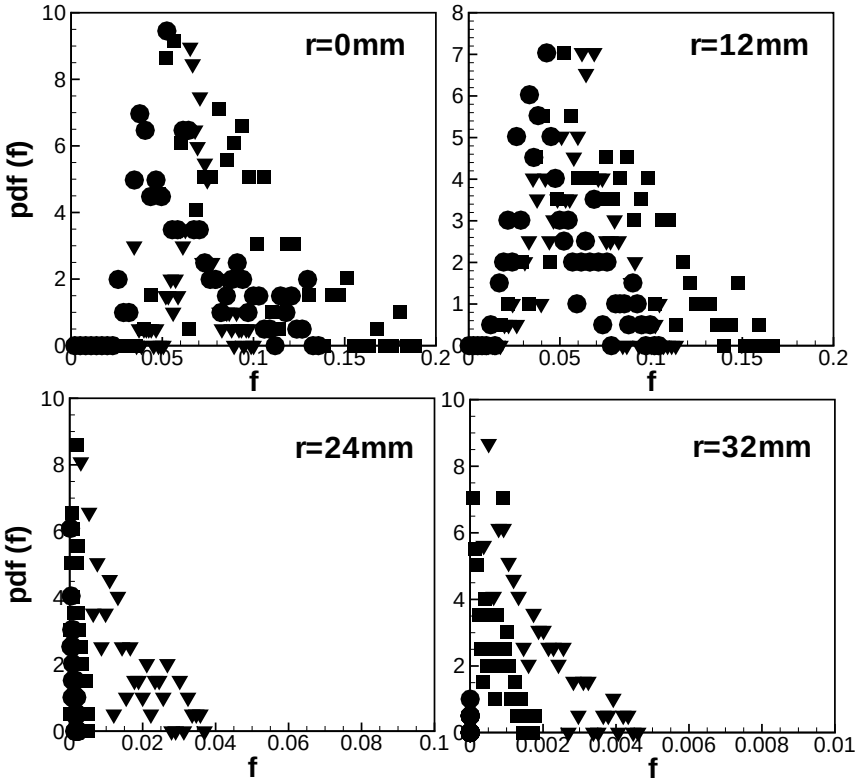

Figure 13: Comparisons of mixture fraction pdfs at x=155mm at equidistant radial locations (a), (b), (c) and (d). Here circles, squares and inverted triangles denote results for swirl numbers 0.5, 0.75 and 1.0

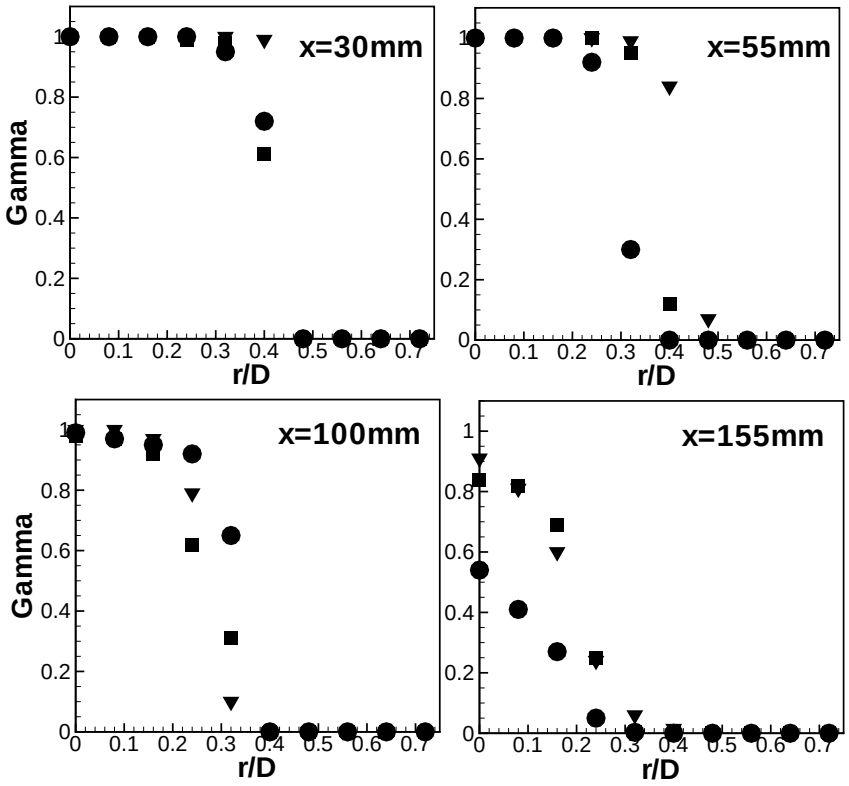

Figure 14: Radial profiles of mixture fraction intermittency at (a) x=30mm, (b) x=55mm, (c) x=100mm and (d) x=155mm. Here circles, squares and inverted triangles denote results for swirl numbers 0.5, 0.75 and 1.0

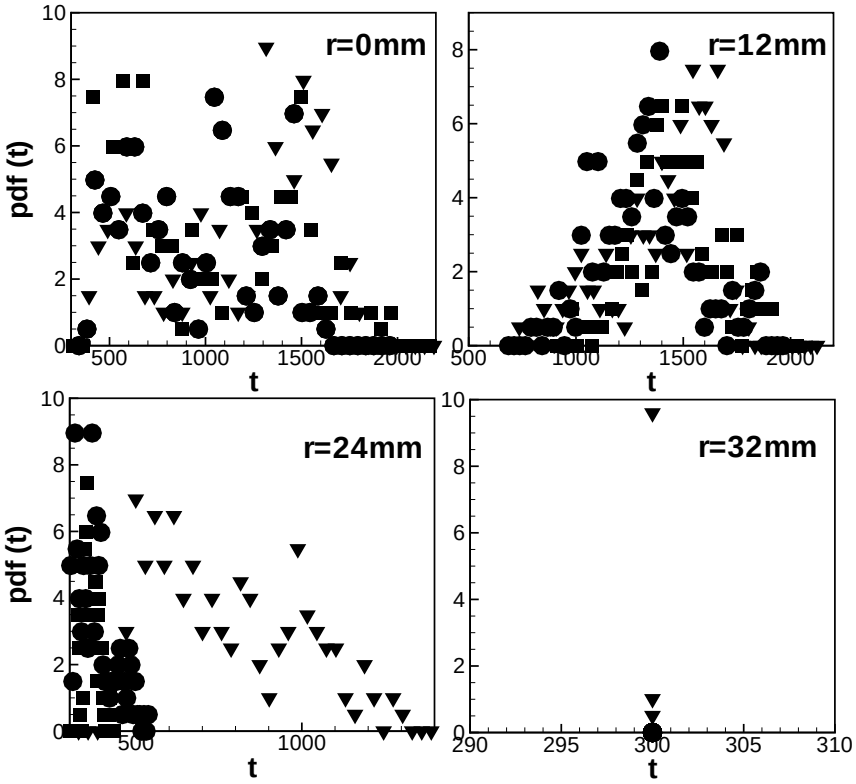

Figure 15: Comparisons of temperature pdfs at x=30mm at equidistant radial locations (a), (b), (c) and (d). Here circles, squares and inverted triangles denote results for swirl numbers 0.5, 0.75 and 1.0

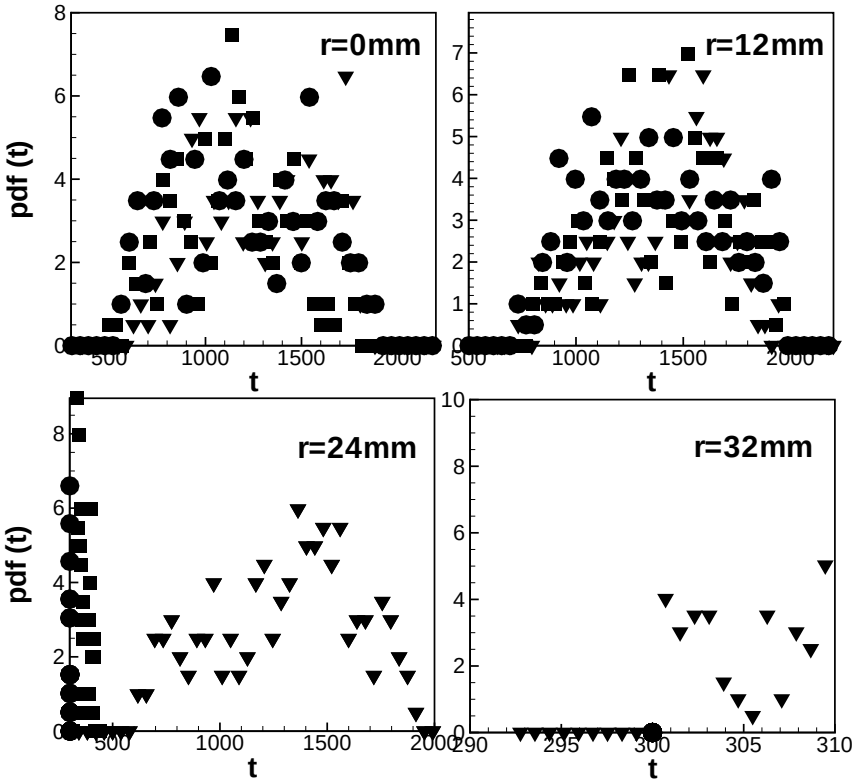

Figure 16: Comparisons of temperature pdfs at x=55mm at equidistant radial locations (a), (b), (c) and (d). Here circles, squares and inverted triangles denote results for swirl numbers 0.5, 0.75 and 1.0

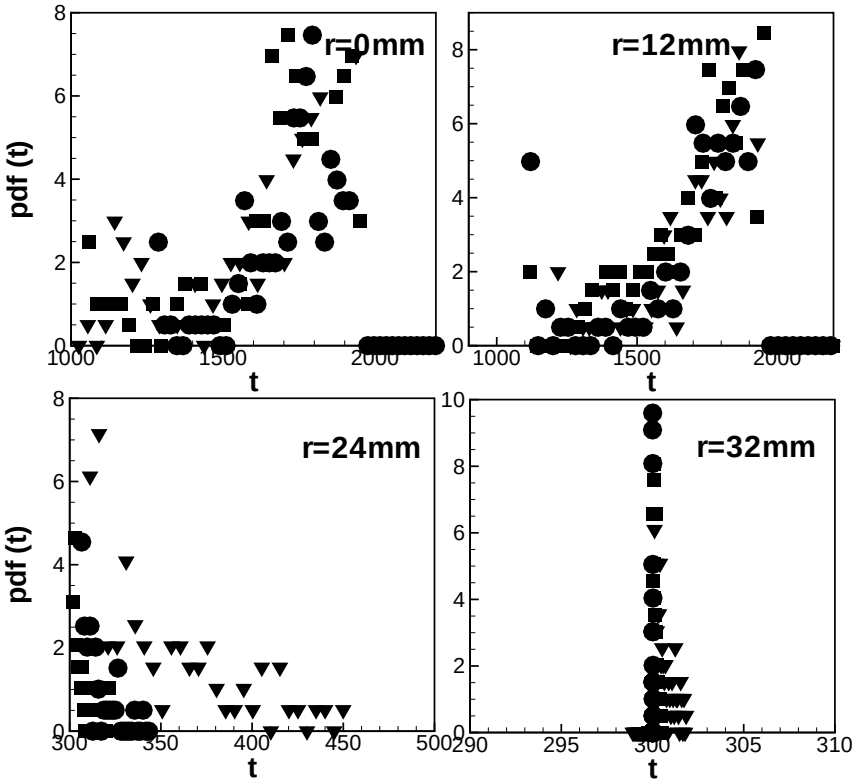

Figure 17: Comparisons of temperature pdfs at x=100mm at equidistant radial locations (a), (b), (c) and (d). Here circles, squares and inverted triangles denote results for swirl numbers 0.5, 0.75 and 1.0

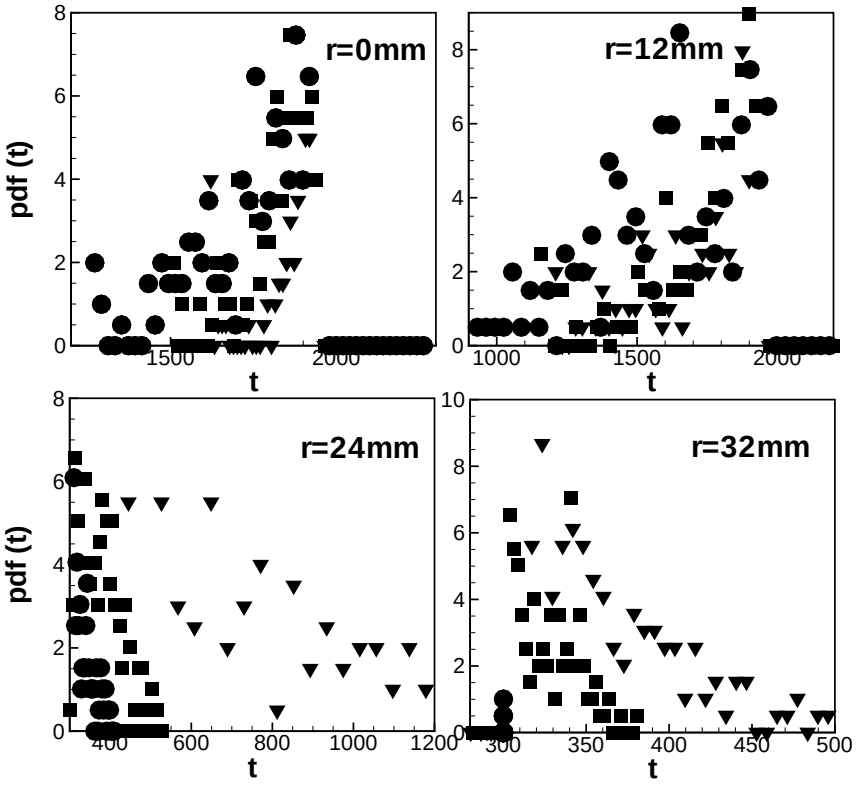

Figure 18: Comparisons of temperature pdfs at x=155mm at equidistant radial locations (a), (b), (c) and (d). Here circles, squares and inverted triangles denote results for swirl numbers 0.5, 0.75 and 1.0

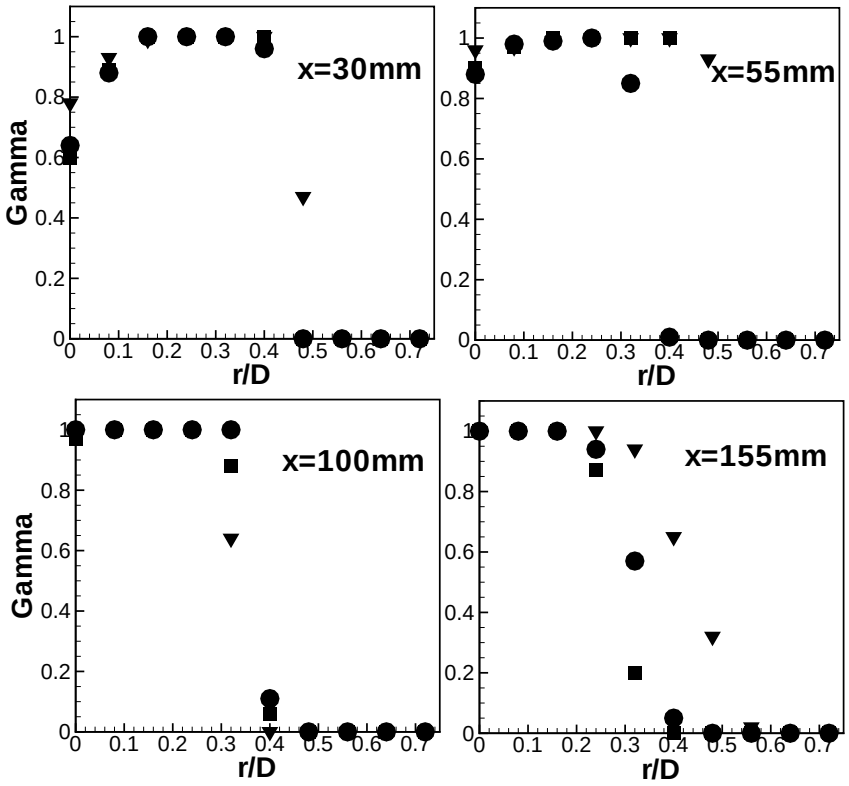

Figure 19: Radial profiles of temperature intermittency at (a) x=30mm, (b) x=55mm, (c) x=100mm and (d) x=155mm. Here circles, squares and inverted triangles denote results for swirl numbers 0.5, 0.75 and 1.0